

# Testing the robustness of the enhanced flow rate of a hopper discharging frictionless hard discs through an adjustable inclusion

Guo-Jie J. Gao,<sup>1,\*</sup> Jerzy Blawdziewicz,<sup>2,3</sup> and Shigenobu Ogata<sup>4,5</sup>

<sup>1</sup>*Department of Mathematical and Systems Engineering,  
Shizuoka University, Hamamatsu, Shizuoka 432-8561, Japan*

<sup>2</sup>*Department of Physics, Texas Tech University, Lubbock, TX 79409-1051, USA*

<sup>3</sup>*Department of Mechanical Engineering, Texas Tech University, Lubbock, TX 79409-1021, USA*

<sup>4</sup>*Department of Mechanical Science and Bioengineering,  
Osaka University, Toyonaka, Osaka 560-8531, Japan*

<sup>5</sup>*Center for Elements Strategy Initiative for Structural Materials (ESISM),  
Kyoto University, Sakyo, Kyoto 606-8501, Japan*

(Dated: July 3, 2022)

Experimentally and numerically, placing a round inclusion near the orifice of a hopper has been shown to locally enhance the gravity-driven hopper flow of monodisperse frictional discs leaving the hopper. To clarify if the enhanced flow rate is related to the friction between different objects in the system, the disc dispersity, or the inclusion geometry, we developed molecular dynamics (MD) simulations to measure the flow rate of monodisperse or bidisperse frictionless discs passing through a round or a flat inclusion. The locally enhanced flow rates still appear in all cases, which indicates that the three tested factors are not the fundamental reason causing this phenomenon. We propose a hypothesis, supported by simulation evidence, based on the flow rate difference between its value around the inclusion and its maximum with no inclusion to explain the enhanced flow rate.

## I. INTRODUCTION

Depending on the external driving forces and container shape, granular materials can behave like solids or liquids. Usually, grains passing through the narrow orifice of a hopper with the orifice/grain diameter ratio greater than six flow continuously, which can be described by the Beverloo equation for funnel flow or by the Johanson equation for mass flow [1–9]. Besides, Using geometrically isotropic grains such as spherical particles [9–15], increasing grain size dispersity [16–18], and introducing inclusions placed near the orifice of a hopper [19, 20] have been shown to globally facilitate granular flowability out of a hopper.

Recently, placing a round inclusion near the orifice of a hopper has been shown to locally speed up the gravity-driven hopper flow rate [21–23]. The flow rate exhibits a peak as the inclusion is placed at an optimal distance away from the orifice of the hopper. Intrigued by this finding, we want to understand what is the roles that the interparticle friction, the particle size dispersity, and the inclusion geometry play in this phenomenon. Using molecular dynamics (MD) method, we studied a frictionless system of monodisperse or bidisperse discs flowing through a round or a flat inclusion placed near the orifice of a hopper and measured the gravity-driven flow rate in terms of number of discs out of the hopper per unit time. We still observe local flow rate peaks in all situations. Our results suggest that neither the friction, nor the particle dispersity, nor the inclusion geometry acts as the fundamental factor responsible for the enhanced hopper

flow rate. We therefore propose a hypothesis, supported by simulation evidence, which says that the locally enhanced flow rate can be simply explained by the flow rate difference between its value around the inclusion and its maximum with no inclusion. The hypothesis can reasonably predict where the local flow rate peak happens without resorting to the continuum theory of granular hopper flow.

Below we elaborate on our MD method for gravity-driven hopper flow in section II, followed by quantitative results of investigating the hopper flow rates using three simulation conditions in section III. We conclude our study in section IV.

## II. NUMERICAL SIMULATION METHOD

### A. System geometry

We develop molecular dynamics (MD) simulations to study the gravity-driven discharging of monodisperse or 50-50 bidisperse frictionless circular dry particles from a geometrically symmetric hopper with a height  $L$  and a hopper angle  $\theta = 0.4325$  radians, as shown schematically in Fig. 1. An inclusion of size  $D = 0.112L$  along its longest dimension is placed on the symmetric axis of the hopper and away from its orifice by a controllable distance  $H$ . The inclusion could be one disc of diameter  $D$  or three horizontally-aligned discs, each of diameter  $D/3$ , to resemble a flat inclusion. The disc diameter  $d$  of the monodisperse system is about the same as the large disc diameter  $d_l$  of the bidisperse system, with  $L/d = 83$  and  $L/d_l = 82.857$ . The size ratio between the inclusion and a particle is  $D/d = 9.296$  and  $D/d_l = 9.28$ . In the bidisperse system, the diameter ratio between large

\* koh.kokketsu@shizuoka.ac.jp, gjgao@gmail.com

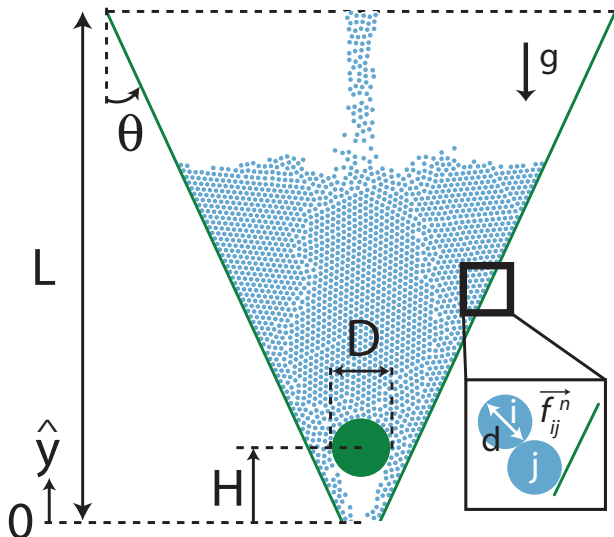


FIG. 1. The simulation setup modeling steady gravity-driven hopper flow of frictionless discs (blue circles) of diameter  $d$ . An inclusion (green circle) of diameter  $D$  sits at a height  $H$  above the orifice of a symmetric hopper (green straight lines) with a height  $L$  and a hopper angle  $\theta$ . Gravity  $g$  is in the downward ( $-y$ ) direction. The inset shows the discs are subject to interparticle normal forces only.

and small discs is  $d_l/d_s = 1.4$  to prevent artificial crystallization in a two dimensional environment. There are  $N$  discs in the system, where  $N = 2048$  and  $2712$  for the monodisperse and bidisperse systems, respectively. We do so to make sure that the particles in each system fill the hopper up to about  $2/3$  of its height while a steady hopper flow is maintained without particles piling up to reach the top simulation border of the hopper. To maintain a constant number of particles  $N$  in our hopper flow simulation, a particle dropping out of the hopper will reenter the hopper from its top border by artificially shifting the particle's vertical ( $y$ ) position by a distance  $L$  while keeping its horizontal ( $x$ ) position and velocities in both directions unchanged.

### B. Interactions between objects within the system

In our simulation, where initially orderly placed discs fall under gravity and the system eventually reaches a steady state of gravity-driven hopper flow, each particle  $i$  obeys the Newton's translational equation of motion

$$\vec{F}_i = \vec{F}_i^{\text{int}} + \vec{F}_i^W + \vec{F}_i^I + \vec{F}_i^G = m_i \vec{a}_i, \quad (1)$$

where  $\vec{F}_i$  is the total force acting on particle  $i$  with mass  $m_i$  and acceleration  $\vec{a}_i$ .  $\vec{F}_i^{\text{int}}$ ,  $\vec{F}_i^W$ ,  $\vec{F}_i^I$  and  $\vec{F}_i^G$  are forces acting on particle  $i$  from its contact neighbors, the hopper wall, the inclusion and gravity, respectively.

The simplest model of frictionless granular materials considers only the interparticle normal forces [24]. The

interparticle force  $\vec{F}_i^{\text{int}}$  on particle  $i$  having  $N_c$  contact neighbors can be expressed as

$$\vec{F}_i^{\text{int}} = \sum_{j \neq i}^{N_c} [\vec{f}_{ij}^n(r_{ij}) + \vec{f}_{ij}^d(r_{ij})], \quad (2)$$

where  $\vec{f}_{ij}^n(r_{ij})$  and  $\vec{f}_{ij}^d(r_{ij})$  are the interparticle normal force and normal damping force defined in Eqn.(3) and Eqn.(4), respectively.

Specifically, we assume that each frictionless particle  $i$  is subjected to a finite-range, purely repulsive linear spring normal force from its contact neighbor  $j$

$$\vec{f}_{ij}^n(r_{ij}) = \frac{\epsilon}{d_{ij}^2} \delta_{ij} \Theta(\delta_{ij}) \hat{r}_{ij}, \quad (3)$$

where  $r_{ij}$  is the separation between disc particles  $i$  and  $j$ ,  $\epsilon$  is the characteristic elastic energy scale,  $d_{ij} = (d_i + d_j)/2$  is the average diameter,  $\delta_{ij} = d_{ij} - r_{ij}$  is the interparticle overlap,  $\Theta(x)$  is the Heaviside step function, and  $\hat{r}_{ij}$  is the unit vector connecting particle centers.

Similarly, we consider only the interparticle normal damping force proportional to the relative velocity between particles  $i$  and  $j$

$$\vec{f}_{ij}^d(r_{ij}) = -b \Theta(\delta_{ij}) (\vec{v}_{ij} \cdot \hat{r}_{ij}) \hat{r}_{ij}, \quad (4)$$

where  $b$  is the damping parameter,  $\vec{v}_{ij}$  is the relative velocity between the two particles. The normal damping force results in deduction of the kinetic energy of the system after each pairwise collision.

The interaction force  $\vec{F}_i^W$  between particle  $i$  and a hopper wall has an analogous form to the interparticle interaction  $\vec{F}_i^{\text{int}}$  with  $\epsilon^W = 2\epsilon$ , which means when a particle hits a wall, it experiences a repulsive force as if it hit another mirrored self on the other side of the wall. The particle-inclusion interaction force  $\vec{F}_i^I$  also has the same analogous form, and its value stays zero if the hopper contains no inclusion. Finally,  $\vec{F}_i^G = -m_i g \hat{y}$ , where  $g$  is the gravitational constant, and  $\hat{y}$  is the unit vector in the upward direction. There is no tangential interaction on particles in this model, and therefore the Newton's rotational equation of motion is automatically satisfied.

The MD simulations in this study use the diameter  $d$  and mass  $m$  of the monodisperse particles and the interparticle elastic potential amplitude  $\epsilon$  as the reference length, mass, and energy scales, respectively. For the bidisperse system,  $d_s$  and mass  $m_s$  of the small particles separately replace  $d$  and  $m$ . To maintain a steady hopper flow without particles piling up to the upper border of the hopper and bringing in unwanted boundary effects, we use the dimensionless damping parameter to  $b^* = db/\sqrt{m\epsilon} = 0.5$ , the dimensionless gravity  $g^*$  to  $10^{-4}$ , and a dimensionless time step  $dt^* = dt/d\sqrt{m/\epsilon}$  to  $10^{-3}$  throughout this study.

### C. Measuring the hopper flow rate

To measure the hopper flow rate while the inclusion is placed at a given value of  $H$  above the hopper orifice, we initiate one simulation with orderly arranged particles. We also randomized size identities for the bidisperse system. Then we wait for a time interval  $\Delta t^* = 5 \times 10^4$  until the system forgets the initial arrangement and reaches a steady state of gravity-driven hopper flow. After that, we count the number of particles passing the orifice of the hopper within another  $\Delta t^*$ . For each value of  $H$ , we use 18 different initial conditions to evaluate the average and the variance of the actual flow rate  $J_a$  in terms of number of particles leaving the hopper per unit time. We define  $J_o$  as the value of  $J_a$  while the hopper contains no inclusion.

## III. RESULTS AND DISCUSSIONS

Our investigation contains two parts: A) To understand the influence of the interparticle friction on the locally enhanced hopper flow rate, we compare our frictionless results of the same hopper geometry with the frictional data, where monodisperse disc particles passing through a round inclusion [23]. B) To understand the contribution of the inclusion geometry or particle dispersity, we measured the flow rates of frictionless discs in three cases: (1) monodisperse discs and a round inclusion, (2) monodisperse discs and a flat inclusion, and (3) 50-50 bidisperse discs and a round inclusion. The results are shown in Fig. 2 below, where the actual flow rate  $J_a$ , normalized by  $J_o$ , is plotted against the normalized inclusion position  $H/d$  or  $H/d_l$  for the monodisperse or bidisperse system.  $J_o$  is  $\approx 0.0319$  for the monodisperse system, and its value increases by about 27% to  $\approx 0.0406$  for the bidisperse system.

### A. Comparing with the frictional data

Unlike their frictional counterparts, frictionless particles start to flow earlier and the normalized flow rate  $J_a/J_o$  already reaches about 60% or higher as the inclusion is lifted to about ten-particle high ( $H/d \approx 10$ ) above the hopper orifice. On the other hand, the frictional normalized flow rate is only slightly above zero at a similar  $H/d$ . The local peak value of frictional  $J_a/J_o$  can be greater than unity, while all three frictionless peaks have  $J_a/J_o$  below unity with lower heights.

### B. Comparing between frictionless cases

We find that the hopper flow rate can be locally enhanced in all three frictionless cases, that is,  $J_a/J_o$  exhibits a local peak while the inclusion is lifted to about eleven to twelve particles high ( $H/d \approx 11$  to 12) above

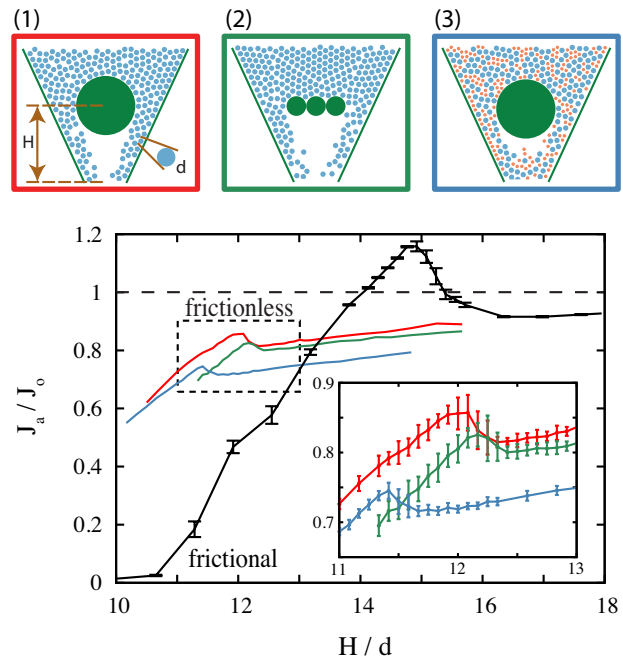


FIG. 2. Averaged frictionless flow rates  $J_a/J_o$  under different simulation setup: (1) monodisperse discs and a round inclusion (red); (2) monodisperse discs and a near flat inclusion (green); (3) bidisperse discs and a round inclusion (blue). The inset zooms in the dashed area. Each data point is obtained using 18 different initial conditions. A simulation snapshot of each frictionless setup is shown on the top with corresponding border color. The frictional flow rate of monodisperse discs and a round inclusion (black) is reproduced from Fig. 3(b) in Ref. [23] for a quantitative comparison.

the orifice of the hopper. Among the three cases, the bidisperse one with a larger  $J_o$  exhibits its flow rate peak at  $H/d \approx 11.4$ , earlier than the other two monodisperse cases. Between the two monodisperse cases with a round and a flat inclusion, the round inclusion blocks the hopper flow less than the flat one, and the system shows a peak slightly earlier at  $H/d \approx 12$ .

### C. Mechanism for the locally enhanced flow rate

Our results clearly show that none of the interparticle friction, the inclusion geometry, and the particle dispersity is directly responsible for the locally enhanced flow rate, though they do affect where the flow rate peak occurs. To better understand what causes the enhanced flow rate, we propose a hypothesis explaining the phenomenon based on the flow rate difference between its value  $J_i$  around the inclusion and its maximum  $J_o$  while with no inclusion, as shown schematically in Fig. 3(a). Here we measure  $J_i$  at the same vertical height where the center of the inclusion locates, that is, the height  $H$  above the orifice of the hopper. Practically,  $J_i$  can be measured by slicing off the part of the hopper below the center of

the inclusion so that the removed piece of hopper has no effect on  $J_i$ .

Our hypothesis states that when the inclusion locates closer to the hopper orifice,  $J_i$  is lower than  $J_o$ , which corresponds to a fluidized flow regime as shown in Fig. 3(a1), and we should observe a monotonically increase of the actual flow rate  $J_a$ . On the other hand, when the inclusion is placed further away from the orifice, the two internal passages between the inclusion and the two hopper walls on its either side together can allow  $J_i$  to become higher than  $J_o$ , which creates a clogging flow regime, as shown in Fig. 3(a2). During the transition from the fluidized regime to the clogging regime,  $J_a$  can be locally boosted due to a greater-than-unity  $J_i/J_o$  that cannot be smoothly constrained by the hopper until the flow leaves its orifice and therefore exhibits a local peak.  $J_a$  then increases again as the position  $H$  of the inclusion becomes higher until eventually reaches its maximum  $J_o$ .

To offer simulation evidence for our hypothesis, we show  $J_o$ ,  $J_i$  and  $J_a$  of the frictionless case (1) of monodisperse discs and a round inclusion as an example. The results are shown in Fig. 3(b). To numerically measure  $J_i$ , we put particles dropping below  $H$  back the top of the hopper but slightly lower than its top border by a distance of  $0.1L$ . Besides, we place a lid with a dimensionless damping parameter  $b_l^* = 50b^*$  at the top border of the hopper to prevent fast-flying particles from escaping the simulation domain and to conserve the total number of particles  $N$  in the system. As expected, we observe a monotonic increase of  $J_a$  while  $J_i$  is below  $J_o$ . A peak of  $J_a$  occurs soon after  $J_i$  becomes higher than  $J_o$ .

#### IV. CONCLUSIONS

Using frictionless MD simulations, we tested the significance of the interparticle friction, the inclusion geometry and the particle dispersity on the enhanced hopper flow rate, found in frictional systems where discs passing through a round inclusion. Our results show that none the three parameters has fundamental contribution to the focused phenomenon. We therefore propose a hypothesis, based on the flow rate difference between its value  $J_i$  around the inclusion and its maximum  $J_o$  without an inclusion, to explain the local peak of the actual flow rate  $J_a$ : when  $J_i$  becomes higher than  $J_o$ ,  $J_a$  can be locally boosted and shows a peak. We support our hypothesis with simulation evidence.

Although the hypothesis can succinctly explain the locally enhanced flow rate, it still does not completely exclude other factors such as the interparticle collaborative motion, feasible by the Newtonian dynamics, from contributing to the phenomenon. For example, a group of particles can crystallize above the inclusion, and there also could be coordinative motion between particles and the hopper walls below the inclusion before these particles leave the hopper. To differentiate these factors, one approach is to prepare a Tetris model which creates an

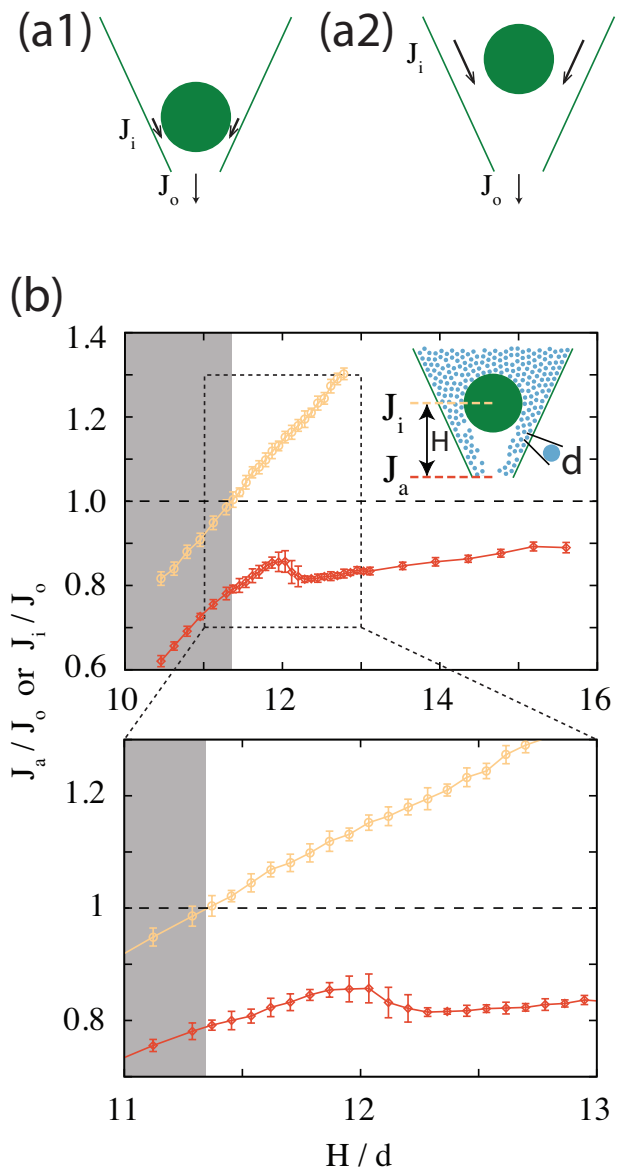


FIG. 3. (a1) Schematic explaining a fluidized flow regime where the flow rate  $J_i$  around the inclusion is smaller than its maximum  $J_o$  with no inclusion. (a2) Schematic explaining a clogging flow regime where  $J_i > J_o$ . (b) Averaged flow rates,  $J_i$  (orange) and  $J_a$  (red), normalized by  $J_o$  for the frictionless system with monodisperse disc particles and a round inclusion. Each data point is obtained using 18 different initial conditions. A zoomed-in plot at the bottom emphasizes the transition from  $J_i < J_o$  (fluidized flow regime, shaded) to  $J_i > J_o$  (clogging flow regime, unshaded), followed by the occurrence of a local peak of  $J_a$ .

artificial hopper flow whose  $J_i$  is low initially and gradually becomes higher than  $J_o$  as a function of the inclusion height  $H$ , like in the experiments and the MD models. In the Tetris model, particles move sequentially according to predefined probability functions without communicating through the Newton's equations of motion. One could measure  $J_a$  of the Tetris model to see if it still shows a

local peak. If a peak of  $J_a$  still occur, then it serves as an indisputable evidence that the interparticle collaborative motion and the Newtonian dynamics behind it are not essential for this phenomenon. We will pursue this model in our next investigation.

## V. ACKNOWLEDGMENTS

GJG gratefully acknowledges financial support from startup funding of Shizuoka University (Japan).

- 
- [1] W. A. Beverloo, H. A. Leninger, and J. van de Valde, *Chem. Eng. Sci.* **15**, 260 (1961).
  - [2] J. R. Johanson, *Trans. Min. Engrs. AIME* **232**, 69 (1965).
  - [3] A. Janda, I. Zuriguel, and D. Maza, *Phys. Rev. Lett.* **108**, 248001 (2012).
  - [4] H. M. Jaeger and S. R. Nagel, *Science* **255**, 1523 (1992).
  - [5] K. Hutter and K. R. Rajagopal, *Continuum Mech. Thermodyn.* **6**, 81 (1994).
  - [6] H. M. Jaeger, S. R. Nagel, and R. P. Behringer, *Rev. Mod. Phys.* **68**, 1259 (1996).
  - [7] C. S. Campbell, *Powder Technol.* **162**, 2006 (2006).
  - [8] P. Jop, Y. Forterre, and O. Pouliquen, *Nature* **441**, 727 (2006).
  - [9] C. C. Thomas and D. J. Durian, *Phys. Rev. E* **87**, 052201 (2013).
  - [10] G. W. Baxter, R. P. Behringer, T. Fagert, and G. A. Johnson, *Phys. Rev. Lett.* **62**, 2825 (1989).
  - [11] P. W. Cleary and M. L. Sawley, *Appl. Math. Model.* **26**, 89 (2002).
  - [12] C. Wu and A. C. F. Cocks, *Mechanics of Materials* **38**, 304 (2006).
  - [13] P. W. Cleary, *Powder Technol.* **179**, 144 (2008).
  - [14] F. Y. Fraige, P. A. Langston, and G. Z. Chen, *Powder Technol.* **186**, 224 (2008).
  - [15] D. Höhner, S. Wirtz, and V. Scherer, *Powder Technol.* **226**, 16 (2012).
  - [16] A. V. Potapov and C. S. Campbell, *Phys. Fluids* **8**, 2884 (1996).
  - [17] C. Denniston and H. Li, *Phys. Rev. E* **59**, 3289 (1999).
  - [18] B. Remy, J. G. Khinast, and B. J. Glasser, *Chem. Eng. Sci.* **66**, 1811 (2011).
  - [19] U. Tüzün and R. M. Nedderman, *Chem. Eng. Sci.* **40**, 325 (1985).
  - [20] S. C. Yang and S. S. Hsiau, *Powder Technol.* **120**, 244 (2001).
  - [21] I. Zuriguel, A. Janda, A. Garcimartín, C. Lozano, R. Arévalo, and D. Maza, *Phys. Rev. Lett.* **107**, 278001 (2011).
  - [22] C. Lozano, A. Janda, A. Garcimartín, D. Maza, and I. Zuriguel, *Phys. Rev. E* **86**, 031306 (2012).
  - [23] F. Alonso-Marroquin, S. I. Azeezullah, S. A. Galindo-Torres, and L. M. Olsen-Kettle, *Phys. Rev. E* **85**, 020301 (2012).
  - [24] G. J. Gao, J. Blawdziewicz, C. S. O'Hern, and M. D. Shattuck, *Phys. Rev. E* **80**, 061304 (2009).